Archives of Biochemistry and Biophysics 528 (2012) 32–44

Contents lists available at SciVerse ScienceDirect

Archives of Biochemistry and Biophysics

journal homepage: www.elsevier.com/locate/yabbi

Acidic pH promotes oligomerization and membrane insertion of the BclXL apoptotic repressor

Vikas Bhat [a], Dmitry Kurouski [b], Max B. Olenick [a], Caleb B. McDonald [a], David C. Mikles [a], Brian J. Deegan [a], Kenneth L. Seldeen [a], Igor K. Lednev [b], Amjad Farooq [a,*]

[a] Department of Biochemistry and Molecular Biology, Leonard Miller School of Medicine, University of Miami, Miami, FL 33136, USA
[b] Department of Chemistry, University at Albany, SUNY, Albany, NY 12222, USA

ARTICLE INFO

Article history:
Received 3 July 2012
and in revised form 19 August 2012
Available online 30 August 2012

Keywords:
Protein oligomerization
Molten globule
Membrane insertion
Ligand binding
Allosteric regulation

ABSTRACT

Solution pH is believed to serve as an intricate regulatory switch in the induction of apoptosis central to embryonic development and cellular homeostasis. Herein, using an array of biophysical techniques, we provide evidence that acidic pH promotes the assembly of BclXL apoptotic repressor into a megadalton oligomer with a plume-like appearance and harboring structural features characteristic of a molten globule. Strikingly, our data reveal that pH tightly modulates not only oligomerization but also ligand binding and membrane insertion of BclXL in a highly subtle manner. Thus, while oligomerization and the accompanying molten globular content of BclXL is least favorable at pH 6, both of these structural features become more pronounced under acidic and alkaline conditions. However, membrane insertion of BclXL appears to be predominantly favored under acidic conditions. In a remarkable contrast, while ligand binding to BclXL optimally occurs at pH 6, it is diminished by an order of magnitude at lower and higher pH. This reciprocal relationship between BclXL oligomerization and ligand binding lends new insights into how pH modulates functional versatility of a key apoptotic regulator and strongly argues that the molten globule may serve as an intermediate primed for membrane insertion in response to apoptotic cues.

Introduction

The Bcl2 family of proteins plays a central role in coupling apoptotic stimuli to the removal of damaged and unwanted cells during physiological processes such as embryonic development and cellular homeostasis [1–8]. The Bcl2 proteins can be divided into three major groups: activators, effectors and repressors. Activators such as Bid and Bad belong to the BH3-only proteins, where BH3 is the Bcl2 homology 3 domain. Effectors such as Bax and Bak contain the BH3–BH1–BH2–TM modular architecture, where TM is the transmembrane domain located C-terminal to Bcl2 homology domains BH3, BH1 and BH2. Repressors such as Bcl2, BclXL and BclW are characterized by the BH4–BH3–BH1–BH2–TM modular organization, with an additional N-terminal Bcl2 homology 4 domain. According to one school of thought, the apoptotic fate, or the decision of a cell to continue to live or pull the trigger to commit suicide, is determined by the cellular ratio of activator, effector and repressor molecules [9,10]. In quiescent and healthy cells, the effectors are maintained in an inactive state via complexation with repressors. Upon receiving apoptotic cues, in the form of DNA damage and cellular stress, the activators are stimulated and compete with effectors for binding to the repressors and, in so doing, not only do they neutralize the anti-apoptotic action of repressors but also unleash the pro-apoptogenicity of effectors. The effectors subsequently initiate apoptotic cell death by virtue of their ability to insert into the mitochondrial outer membrane (MOM)[1] resulting

* Corresponding author. Fax: +1 305 243 3955.
E-mail address: amjad@farooqlab.net (A. Farooq).

[1] *Abbreviations used:* ALS, analytical light scattering; ANS, 8-anilinonaphthalene-1-sulfonate; Bad, Bcl2-associated death (promoter); Bak, Bcl2 (homologous) antagonist/killer; Bax, Bcl2-associated X (protein); Bcl2, B-cell lymphoma 2; BclXL, B-cell lymphoma extra large; BclXL_transTM, BclXL homodimer in which the TM domain of one monomer occupies the canonical hydrophobic groove within the other monomer and vice versa in a domain-swapped trans-fashion; BclXL_runawayTM, BclXL oligomer in which the TM domain of one monomer occupies the canonical hydrophobic groove within the adjacent monomer and the TM domain of this second monomer in turn occupies the canonical hydrophobic groove within the third monomer in a runaway domain-swapping fashion; BH1, Bcl2 homology 1 (domain); BH2, Bcl2 homology 2 (domain); BH3, Bcl2 homology 3 (domain); BH4, Bcl2 homology 4 (domain); Bid, BH3-interacting domain (death agonist); Bid_BH3, 20-mer peptide derived from the BH3 domain of Bid; CAPS, *N*-cyclohexyl-3-aminopropanesulfonic acid; CD, circular dichroism; DHPC, 1,2-dihexanoyl-*sn*-glycero-3-phosphocholine; DLS, dynamic light scattering; ITC, isothermal titration calorimetry; LIC, ligation-independent cloning; MD, molecular dynamics; MM, molecular modeling; MOM, mitochondrial outer membrane; SEC, size-exclusion chromatography; SEM, scanning electron microscopy; SLS, static light scattering; SSF, steady-state fluorescence; TOCL, 1,1′,2,2′-tetraoleoyl cardiolipin (1′,3′-bis[1,2-dioleoyl-*sn*-glycero-3-phospho]-*sn*-glycerol).

0003-9861/$ - see front matter © 2012 Elsevier Inc. All rights reserved.
http://dx.doi.org/10.1016/j.abb.2012.08.009

in the formation of mitochondrial pores in a manner akin to the insertion of bacterial toxins such as colicins and diphtheria [11–15]. This leads to the release of apoptogenic factors such as cytochrome *c* and Smac/Diablo from mitochondria into the cytosol. Subsequently, rising levels of apoptogenic factors in the cytosol switch on aspartate-specific proteases termed caspases, which in turn, demolish the cellular architecture by cleavage of proteins culminating in total cellular destruction.

Despite their low sequence convergence, all members of Bcl2 family share a remarkably conserved 3D topological fold characterized by a central predominantly hydrophobic α-helical hairpin "dagger" (α5 and α6) surrounded by a "cloak" comprised of six amphipathic α-helices (α1–α4 and α7–α8) of varying lengths [16]. A prominent feature of repressors is that they contain what has come to be known as the "canonical hydrophobic groove", formed by the juxtaposition of α2–α5 helices, that serves as the docking site for the BH3 domain (α2 helix) of activators and effectors. Additionally, the effectors and repressors also contain a C-terminal hydrophobic α-helix termed α9, or more commonly the TM domain, because it allows these members of the Bcl2 family to localize to MOM upon apoptotic induction [17–19]. The "cloak and dagger" structural topology of Bcl2 members is the hallmark of their functional duality in that they are able to co-exist as "soluble factors" under quiescent cellular state and as "membrane channels" upon apoptotic induction. Notably, the hydrophobic dagger not only provides the bulk of the thermodynamic force in driving the water–membrane transition of various Bcl2 members upon apoptotic induction but also directly participates in the formation of mitochondrial pores that provide a smooth channel for the exit of apoptogenic factors. In particular, the water–membrane transition of effectors and repressors is believed to be driven by acidic pH, and optimally occurs at around pH 4, in a manner akin to pore formation by the bacterial toxins [20–24,14,25,26]. The acidic pH destabilizes the solution conformation of these proteins while at the same time inducing the formation of molten globule, which is believed to serve as an intermediate for subsequent insertion into membranes [27,11,28,29]. It should be noted that the molten globule is a partially disordered conformation which contains a native-like secondary structure but without the tightly-packed hydrophobic core comprised of nonpolar residues [30–33]. Importantly, several lines of evidence suggest the formation of a pH gradient across the mitochondria, accompanied by the alkalinization of mitochondrial matrix and acidification of the cytosol, upon the induction of apoptosis [34–39]. This observation further corroborates the role of acidic pH in driving apoptotic machinery.

We have previously shown that BclXL displays the propensity to oligomerize in solution and that such oligomerization is driven by the intermolecular binding of its C-terminal TM domain to the canonical hydrophobic groove in a domain-swapped trans-fashion, whereby the TM domain of one monomer occupies the canonical hydrophobic groove within the other monomer and vice versa [40]. We postulated that such oligomerization serves as a regulatory switch to turn the anti-apoptotic action of BclXL "off" in quiescent cells but "on" in response to apoptotic cues. In an effort to understand how solution pH modulates oligomerization of BclXL and the effect of such oligomerization on subsequent binding of BH3 ligands in the form of activators and effectors and membrane insertion in the context of apoptosis, we undertook the present study. Herein, we provide evidence that acidic pH promotes the assembly of BclXL apoptotic repressor into a megadalton oligomer with a plume-like appearance and harboring structural features characteristic of a molten globule. Strikingly, our data reveal that pH tightly modulates not only oligomerization but also ligand binding and membrane insertion of BclXL in a highly subtle manner. Thus, while oligomerization and the accompanying molten globular content of BclXL is least favorable at pH 6, both of these structural features become more pronounced under acidic and alkaline conditions. However, membrane insertion of BclXL appears to be predominantly favored under acidic conditions. In a remarkable contrast, while ligand binding to BclXL optimally occurs at pH 6, it is diminished by an order of magnitude at lower and higher pH. This reciprocal relationship between BclXL oligomerization and ligand binding lends new insights into how pH modulates functional versatility of a key apoptotic regulator and strongly argues that the molten globule may serve as an intermediate primed for membrane insertion in response to apoptotic cues.

Materials and methods

Sample preparation

Full-length human BclXL (residues 1–233) was cloned into pET30 bacterial expression vector with an N-terminal His-tag using Novagen LIC technology, expressed in *Escherichia coli* BL21*(-DE3) bacterial strain (Invitrogen) and purified on a Ni–NTA affinity column using standard procedures as described previously [40]. Protein concentration was determined by the fluorescence-based Quant-It assay (Invitrogen) and spectrophotometrically on the basis of an extinction coefficient of 47,440 M^{-1} cm^{-1} calculated for the full-length BclXL using the online software ProtParam at ExPasy Server [41]. Results from both methods were in an excellent agreement. The 20-mer peptide spanning residues 81–100 corresponding to the BH3 domain within human Bid (H_2N–DIIRNIARHLAQVGDSMDRS–COOH), hereinafter referred to as Bid_BH3 peptide, was commercially obtained from GenScript Corporation. The peptide concentration was measured gravimetrically. Mixed TOCL/DHPC bicelles were prepared at a final concentration of 30 mM, at TOCL to DHPC molar ratio of 1:4, by stirring for 2 h at 37 °C in appropriate buffers. Samples of full-length BclXL, Bid_BH3 peptide and TOCL/DHPC bicelles were prepared under various pH conditions using acetate (pH 4.0), phosphate (pH 6.0), Tris (pH 8.0) and CAPS (pH 10.0) buffers. For ITC and ALS measurements, all buffers were made up to a final concentration of 50 mM containing 100 mM NaCl, 1 mM EDTA and 5 mM β-mercaptoethanol at each pH. For DSC, CD, SSF and SEM experiments, all buffers were made up to a final concentration of 50 mM at each pH. All measurements were repeated at least three times.

Isothermal titration calorimetry

Isothermal titration calorimetry (ITC) experiments were performed on a Microcal VP-ITC instrument and data were acquired and processed using the integrated Microcal ORIGIN software. For peptide binding, experiments were initiated by injecting 25 × 10 μl aliquots of 0.5–1 mM of Bid_BH3 peptide from the syringe into the calorimetric cell containing 1.8 ml of 50 μM of BclXL at 25 °C. For membrane insertion, experiments were initiated by injecting 25 × 10 μl aliquots of 50 μM of full-length BclXL from the syringe into the calorimetric cell containing 1.8 ml of 2 mM of TOCL/DHPC at 25 °C. In each case, the change in thermal power as a function of each injection was automatically recorded using the ORIGIN software and the raw data were further processed to yield binding isotherms of heat release per injection either as a function of molar ratio of peptide to BclXL or as a function of molar ratio of BclXL to bicelles. The heats of mixing and dilution were subtracted from the heats of peptide binding or membrane insertion per injection by carrying out a control experiment in which the same buffer in the calorimetric cell was either titrated against the Bid_BH3 peptide or BclXL in an identical manner. The apparent

equilibrium dissociation constant (K_d) and the enthalpic change (ΔH) associated with peptide binding to BclXL or membrane insertion of BclXL at various pH were determined from the non-linear least-squares fit of data to a one-site binding model as described previously [42,40]. The binding free energy change (ΔG) was calculated from the following expression:

$$\Delta G = RT \ln K_d \quad (1)$$

where R is the universal molar gas constant (1.99 cal/K/mol) and T is the absolute temperature. The entropic contribution ($T\Delta S$) to the free energy of binding was calculated from the relationship:

$$T\Delta S = \Delta H - \Delta G \quad (2)$$

where ΔH and ΔG are as defined above.

Analytical light scattering

Analytical light scattering (ALS) experiments were conducted on a Wyatt miniDAWN TREOS triple-angle static light scattering detector and Wyatt QELS dynamic light scattering detector coupled in-line with a Wyatt Optilab rEX differential refractive index detector and interfaced to a Hiload Superdex 200 size-exclusion chromatography column under the control of a GE Akta FPLC system within a chromatography refrigerator at 10 °C. Briefly, BclXL was loaded onto the column at a starting concentration of 50 μM and at a flow rate of 1 ml/min. All data were automatically acquired using the ASTRA software. Notably, the angular- and concentration-dependence of static light scattering (SLS) intensity of BclXL resolved in the flow mode was measured by the Wyatt miniDAWN TREOS detector equipped with three scattering angles positioned at 42°, 90° and 138°. The time- and concentration-dependence of dynamic light scattering (DLS) intensity fluctuation of BclXL resolved in the flow mode was measured by the Wyatt QELS detector positioned at 90° with respect to the incident laser beam. Hydrodynamic parameters M_w (weighted-average molar mass), M_n (number-average molar mass), R_g (weighted-average radius of gyration) and R_h (weighted-average hydrodynamic radius) associated with solution behavior of BclXL were determined by the treatment of SLS data to Zimm model and by non-linear least-squares fit of DLS data to an autocorrelation function as described earlier [43–47,40]. It should be noted that, in both the SLS and DLS measurements, protein concentration (c) along the elution profile of BclXL was automatically quantified in the ASTRA software from the change in refractive index (Δn) with respect to the solvent as measured by the Wyatt Optilab rEX detector using the following relationship:

$$c = (\Delta n)/(dn/dc) \quad (3)$$

where dn/dc is the refractive index increment of the protein in solution.

Differential scanning calorimetry

Differential scanning calorimetry (DSC) experiments were performed on a TA Nano-DSC instrument and data were acquired and processed using the integrated NanoAnalyze software. Briefly, experiments were conducted on 50 μM of BclXL in the 40–120 °C temperature range at a heating rate (dT/dt) of 1 °C/min under an excess pressure of 3 atm. The change in thermal power (dQ/dt) as a function of temperature was automatically recorded using the NanoAnalyze software. Control experiments on the buffers alone were also conducted in an identical manner to generate baselines that were subtracted from the raw data to remove background contribution due to the buffer. The raw data were further processed to yield the melting isotherms of excess heat capacity (C_p) as a function of temperature (T) using the following relationship:

$$C_p = [(dQ/dt)]/[(dT/dt)PV] \quad (4)$$

where P is the initial concentration of protein loaded into the calorimetric cell and V is the effective volume of calorimetric cell (0.3 ml).

Circular dichroism

Circular dichroism (CD) measurements were conducted on a Jasco J-815 spectrometer thermostatically controlled at 25 °C. For far-UV measurements, experiments were conducted on 5 μM of BclXL and data were collected using a quartz cuvette with a 2-mm pathlength in the 190–250 nm wavelength range. For near-UV measurements, experiments were conducted on 30 μM of BclXL and data were collected using a quartz cuvette with a 10-mm pathlength in the 260–340 nm wavelength range. All data were normalized against reference spectra to remove the contribution of buffers. All data were recorded with a slit bandwidth of 2 nm at a scan rate of 10 nm/min. Each data set represents an average of four scans acquired at 0.1 nm intervals. Data were converted to molar ellipticity, [θ], as a function of wavelength (λ) of electromagnetic radiation using the equation:

$$[\theta] = [(10^5 \Delta\varepsilon)/cl]\text{deg cm}^2\ \text{dmol}^{-1} \quad (5)$$

where $\Delta\varepsilon$ is the observed ellipticity in mdeg, c is the peptide or protein concentration in μM and l is the cuvette pathlength in cm.

Steady-state fluorescence

Steady-state fluorescence (SSF) spectra were collected on a Jasco FP-6300 spectrofluorimeter using a quartz cuvette with a 10-mm pathlength at 25 °C. Briefly, experiments were conducted on 5 μM of BclXL alone or in the presence of excess ANS or acrylamide. For intrinsic protein fluorescence measurements, the excitation wavelength was 290 nm and emission was acquired over the 300–500 nm wavelength range. For ANS fluorescence, the excitation wavelength was 375 nm and emission was acquired over the 400–600 nm wavelength range. All data were recorded using a 2.5-nm bandwidth for both excitation and emission. Data were normalized against reference spectra to remove background contribution of appropriate buffers. Fluorescence enhancement (E) of ANS in the presence of BclXL at each pH was calculated from the following equation:

$$E = (\Phi - \Phi_o/\Phi_o) \times 100\% \quad (6)$$

where Φ is the fluorescence yield of ANS in the presence of BclXL and Φ_o is the fluorescence yield of ANS alone at corresponding pH. Fluorescence yield (Φ) is defined as the area integrated under the corresponding SSF spectra. Fluorescence quenching (Q) of BclXL in the presence of acrylamide at each pH was calculated from the following equation:

$$Q = (\Phi_o - \Phi/\Phi_o) \times 100\% \quad (7)$$

where Φ is the fluorescence yield of BclXL in the presence of acrylamide and Φ_o is the fluorescence yield of BclXL alone at corresponding pH.

Scanning electron microscopy

Scanning electron microscopy (SEM) experiments were conducted on a Zeiss Gemini Ultra-55 electron microscope operating at a voltage of 5 kV using the in-lens detector and the images were photographed at a magnification of 50,000×. Data were collected either on 25 μM of BclXL alone and in the presence of 10-M excess of Bid_BH3 peptide or on 10 mM of TOCL/DHPC bicelles alone and in the presence of 25 μM of BclXL at the specified pH. Briefly,

100 μl of each sample was deposited onto a carbon-coated copper grid (200-mesh) and incubated for 5–10 min followed by the removal of excess solution. Grids were negatively stained with 1% uranyl acetate. Excess liquid was wicked away with a filter paper and the grids were allowed to air dry prior to imaging.

Molecular modeling

Molecular modeling (MM) was employed to build structural models of BclXL in two distinct oligomeric conformations, BclXL_transTM and BclXL_runawayTM, using the MODELLER software based on homology modeling in combination with MOLMOL [48,49]. In the BclXL_transTM conformation, the TM domain of one monomer occupies the canonical hydrophobic groove within the other monomer and vice versa in a domain-swapped trans-fashion. In BclXL_runawayTM conformation, the TM domain of one monomer occupies the canonical hydrophobic groove within the adjacent monomer in a head-to-tail manner and the TM domain of this second monomer in turn occupies the canonical hydrophobic groove within the third monomer in a runaway domain-swapping fashion. In each case, solution structures of truncated BclXL in which the TM domain and the α1–α2 loop are missing (PDB# 1BXL), hereinafter referred to as tBclXL, and the full-length Bax in which the TM domain occupies the canonical hydrophobic groove (PDB# 1F16) were used as templates. Additionally, MOLMOL was used to bring various parts and/or monomers into optimal spatial orientations relative to each other in a rigid-body fashion. First, the structural model of full-length BclXL, in which the TM domain occupies the hydrophobic groove within the same molecule in a cis manner, was built using tBclXL (PDB# 1BXL) and Bax (PDB# 1F16) in a multiple-template alignment manner and the residues within the α1–α2 loop were modeled without a template through energy minimization and molecular dynamics simulations. Next, pre-built structural models of two individual monomers of full-length BclXL were brought together in an optimal orientation in MOLMOL such that the α8–α9 loop within one monomer could be domain-swapped with TM domain of the other monomer in a trans (BclXL_transTM) or runaway (BclXL_runaway) fashion without becoming taut. This requirement led to either roughly parallel (BclXL_transTM) or series (BclXL_runaway) orientation of TM domains within each monomer. Finally, the α8–α9 loop preceding the TM domain within each BclXL monomer was excised out and the resulting monomers were used as a template to homology model the structures of BclXL_transTM and BclXL_runawayTM, wherein the residues within the α8–α9 loop within each structural model were modeled without a template through energy minimization and molecular dynamics simulations. For each structural model, a total of 100 atomic models were calculated and the structure with the lowest energy, as judged by the MODELLER Objective Function, was selected for further analysis. The atomic models were rendered using RIBBONS [50]. All calculations and data processing were performed on a Linux workstation equipped with a dual-core processor.

Molecular dynamics

Molecular dynamics (MD) simulations on BclXL as a function of pH were performed with the GROMACS software [51,52] using the integrated OPLS-AA force field [53,54]. Briefly, ionizable residues within the modeled structure of BclXL_transTM dimeric conformation were protonated/deprotonated according to their pK_a values at pH 4.0, 6.0, 8.0 and 10.0 using the H++ server at http://biophysics.cs.vt.edu. Next, the pH-adjusted structures were centered within a cubic box, hydrated using the extended simple point charge (SPC/E) water model [55,56], and the ionic strength of solution was set to 100 mM with NaCl. The hydrated structures were energy-minimized with the steepest descent algorithm prior to equilibration under the NPT ensemble conditions, wherein the number of atoms (N), pressure (P) and temperature (T) within the system were respectively kept constant at ~50,000, 1 bar and 300 K. The Particle–Mesh Ewald (PME) method was employed to compute long-range electrostatic interactions with a 10 Å cut-off [57] and the Linear Constraint Solver (LINCS) algorithm to restrain bond lengths [58]. All MD simulations were performed under periodic boundary conditions (PBC) using the leap-frog integrator with a time step of 2 fs. For the final MD production runs, data were collected every 100 ps over a time scale of 100 ns. All simulations were run on a Linux workstation using parallel processors at the High Performance Computing facility within the Center for Computational Science of the University of Miami.

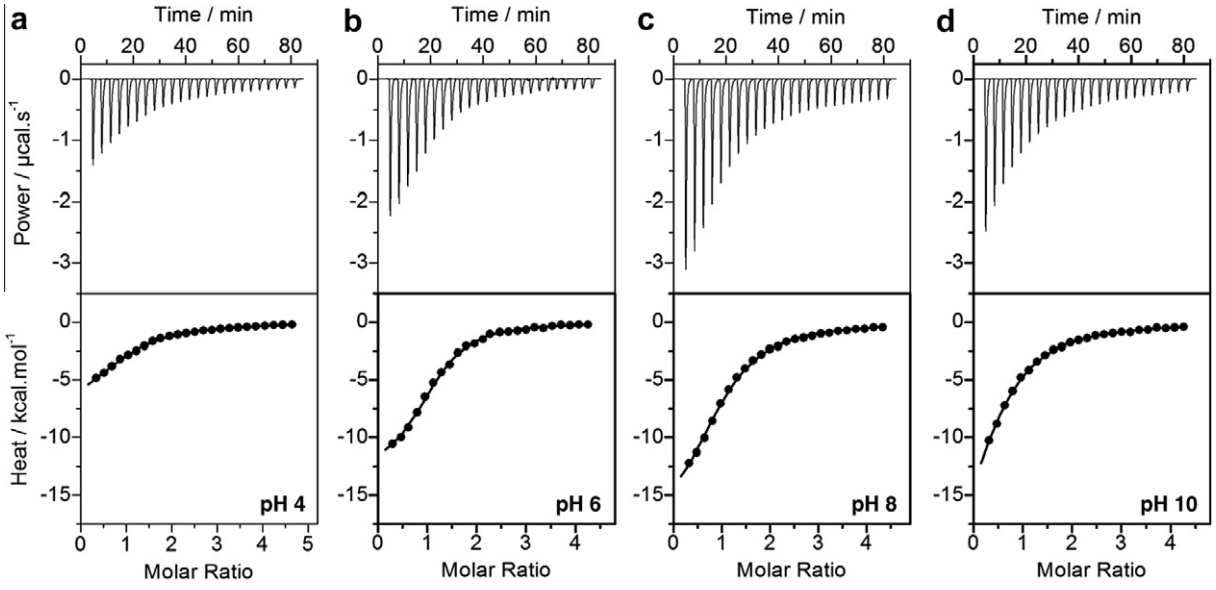

Fig. 1. ITC analysis for the binding of Bid_BH3 peptide to full-length BclXL at pH 4 (a), pH 6 (b), pH 8 (c) and pH 10 (d). The upper panels show raw ITC data expressed as change in thermal power with respect to time over the period of titration. In the lower panels, change in molar heat is expressed as a function of molar ratio of Bid_BH3 peptide to BclXL. The solid lines in the lower panels show non-linear least squares fit of data to a one-site binding model using the ORIGIN software as described earlier [40].

Table 1
pH-dependence of thermodynamic parameters for the binding of Bid_BH3 peptide to full-length BclXL.

	K_d (μM)	ΔH (kcal mol^{-1})	$T\Delta S$ (kcal mol^{-1})	ΔG (kcal mol^{-1})
pH 4	8.30 ± 1.10	−9.09 ± 0.20	−2.15 ± 0.03	−6.94 ± 0.08
pH 6	1.03 ± 0.10	−13.66 ± 0.32	−5.48 ± 0.15	−8.17 ± 0.09
pH 8	10.36 ± 1.52	−18.39 ± 0.53	−11.58 ± 0.29	−6.80 ± 0.04
pH 10	20.51 ± 3.20	−16.54 ± 0.47	−10.13 ± 0.31	−6.40 ± 0.02

All parameters were obtained from ITC measurements. All binding stoichiometries were 1:1 and generally agreed to within ±10%. Errors were calculated from at least three independent measurements. All errors are given to one standard deviation.

Results and discussion

pH modulates ligand binding to BclXL

To understand how solution pH may dictate the binding of BH3 ligands to BclXL, we conducted ITC analysis for the binding of a 20-mer BH3 peptide derived from Bid activator to full-length BclXL as a function of pH (Fig. 1 and Table 1). Our data show that the binding of BH3 peptide to BclXL displays a subtle relationship with increasing pH. Thus, while ligand binding optimally occurs at pH 6, it is diminished by nearly an order of magnitude under acidic conditions (pH 4) to more than an order of magnitude under alkaline environment (pH 8 and 10). The effect of pH on the thermodynamics of ligand binding is also telling. Although binding under all pH conditions analyzed here is favored by enthalpy accompanied by entropic penalty, it is interesting to note that while increasing pH appears to favor enthalpic contributions to the free energy of binding, these favorable changes are largely opposed by equal but opposite entropic factors in agreement with the enthalpy–entropy compensation phenomenon [59–63]. We note that the binding of BH3 peptide to BclXL is not coupled to proton uptake or release since the observed binding enthalpy is independent of the ionization enthalpy of the buffer employed (data not shown). Importantly, we have previously shown that the TM domain reduces the binding of BH3 ligands to BclXL by an order of magnitude by virtue of its ability to bind to the canonical hydrophobic groove in a competitive manner through domain-swapping and thereby promoting the association of BclXL into higher-order oligomers [40]. In light of these observations, our data presented above strongly argue that pH not only modulates ligand binding but that it may also play a key role in the oligomerization of BclXL and that such intramolecular association may in turn modulate ligand binding.

Acidic pH drives the association of BclXL into a megadalton oligomer

To test the hypothesis that the oligomerization of BclXL is pH-dependent, we next analyzed the propensity of BclXL to oligomerize as a function of solution pH using ALS and quantified various physical parameters accompanying its solution behavior from the first principles of hydrodynamics without any assumptions (Fig. 2 and Table 2). Remarkably, our data show that BclXL exclusively associates into a megadalton oligomer comprised of more than 1000 monomeric units (~34,000 kDa), hereinafter referred to as megamer, under acidic conditions (pH 4). At pH 6 and higher, this megamer dissociates and predominantly exists in an equilibrium between monomer (~31 kDa), dimer (~62 kDa), and two higher-order oligomers, herein referred to as multimer (~400 kDa) and polymer (~3500 kDa). However, the ratio of these four species is highly pH-dependent. Thus, while the polymer–multimer–dimer–monomer equilibrium shifts in favor of the smaller species (monomer and dimer) at pH 6, the larger species (multimer and polymer) are favored at pH 8 and pH 10. These salient

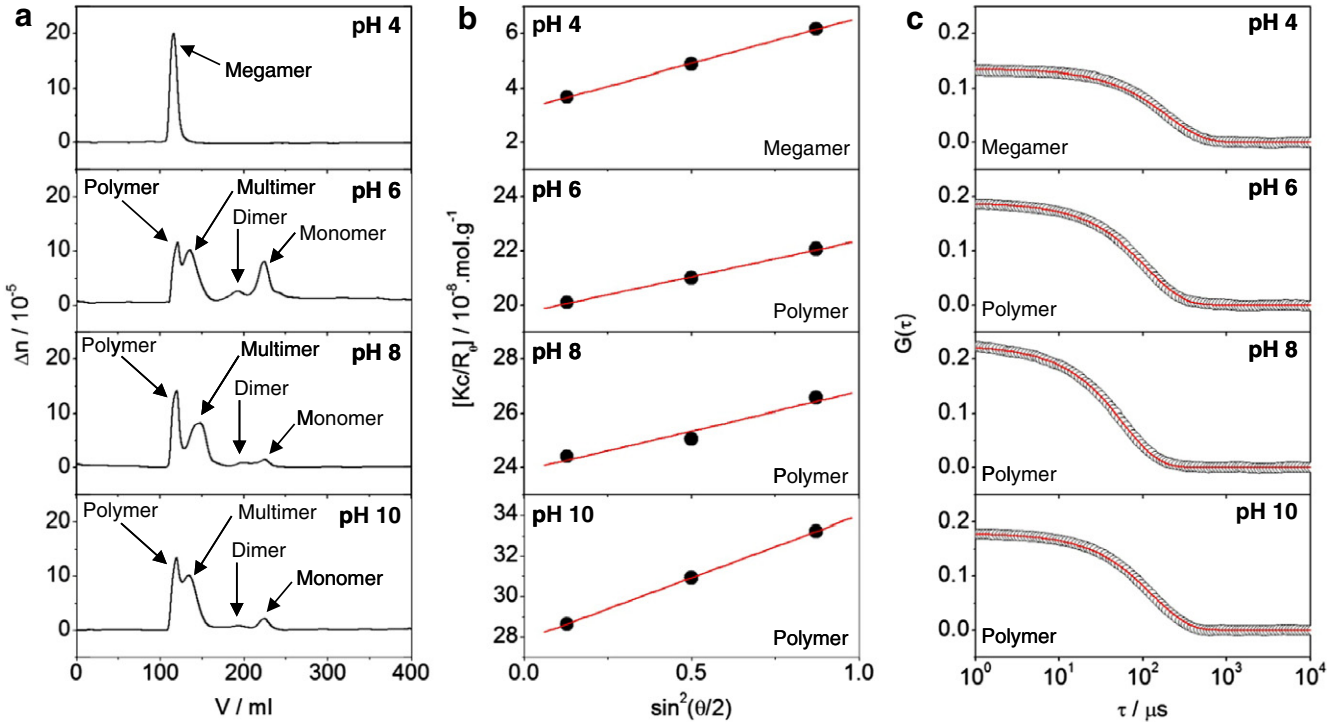

Fig. 2. ALS analysis of full-length BclXL under varying pH as indicated. (a) Elution profiles as monitored by the differential refractive index (Δn) plotted as a function of elution volume (V) at pH 4 (top panel), pH 6 (upper-middle panel), pH 8 (lower-middle panel) and pH 10 (bottom panel). (b) Partial Zimm plots obtained for the oligomeric species as indicated from analytical SLS measurements at pH 4 (top panel), pH 6 (upper-middle panel), pH 8 (lower-middle panel) and pH 10 (bottom panel). The red solid lines through the data points represent linear fits. (c) Autocorrelation function plots obtained for various oligomeric species as indicated from analytical DLS measurements at pH 4 (top panel), pH 6 (upper-middle), pH 8 (lower-middle panel) and pH 10 (bottom panel). The red solid lines represent non-linear least squares fit of data to an autocorrelation function as described earlier [40]. (For interpretation of the references to colour in this figure legend, the reader is referred to the web version of this article.)

Table 2
pH-dependence of hydrodynamic parameters for full-length BclXL.

	Associativity	M_w (kDa)	M_n (kDa)	M_w/M_n	R_g (Å)	R_h (Å)	R_g/R_h	P (%)
pH 4	Megamer	33,805 ± 2821	33,085 ± 2623	1.02 ± 0.01	783 ± 86	324 ± 23	2.40 ± 0.16	100
pH 6	Monomer	32 ± 2	31 ± 2	1.01 ± 0.01	ND	26 ± 1	ND	31
	Dimer	61 ± 3	59 ± 2	1.02 ± 0.01	ND	49 ± 4	ND	11
	Multimer	595 ± 45	577 ± 39	1.03 ± 0.02	141 ± 5	95 ± 3	1.47 ± 0.02	37
	Polymer	3521 ± 292	3101 ± 201	1.13 ± 0.03	230 ± 12	187 ± 9	1.22 ± 0.02	21
pH 8	Monomer	31 ± 1	30 ± 2	1.00 ± 0.00	ND	34 ± 2	ND	7
	Dimer	62 ± 4	61 ± 2	1.01 ± 0.01	ND	48 ± 2	ND	5
	Multimer	364 ± 32	325 ± 33	1.11 ± 0.01	98 ± 4	90 ± 2	1.08 ± 0.02	51
	Polymer	3729 ± 246	3226 ± 236	1.15 ± 0.02	218 ± 12	188 ± 11	1.15 ± 0.03	37
pH 10	Monomer	31 ± 2	32 ± 1	1.00 ± 0.00	ND	32 ± 1	ND	9
	Dimer	61 ± 3	60 ± 3	1.02 ± 0.01	ND	49 ± 3	ND	5
	Multimer	461 ± 21	448 ± 23	1.03 ± 0.01	131 ± 5	108 ± 4	1.21 ± 0.01	50
	Polymer	3189 ± 229	3018 ± 212	1.06 ± 0.02	232 ± 13	202 ± 7	1.14 ± 0.02	36

All parameters were obtained from ALS measurements. The population (P) of each species, as estimated from the integration of corresponding peak in the elution profile (Fig. 2a), is provided in the right-most column. Note that the calculated molar mass of recombinant full-length BclXL from amino acid sequences alone is 31 kDa. Errors were calculated from at least three independent measurements. All errors are given to one standard deviation. Note that the R_g parameter could not be determined (ND) for various species due to their lack of angular-dependence of scattered light.

observations strongly suggest that while pH 6 destabilizes higher-order oligomers of BclXL, alkaline conditions promote association of BclXL into higher-order oligomers and, under acidic conditions, BclXL exclusively associates into a megadalton oligomer. We note that the truncation of the C-terminal TM domain completely abolished oligomerization of BclXL under all pH conditions (data not shown), implying that the intermolecular association of BclXL observed here is driven by the TM domain in agreement with our previous study [40].

In an attempt to gain insights into the conformational heterogeneity of the oligomeric species of BclXL, we also determined the M_w/M_n and R_g/R_h ratios from our hydrodynamic data (Table 2). While the M_w/M_n ratio provides a measure of the macromolecular polydispersity, the R_g/R_h ratio sheds light on the overall macromolecular shape. Our data suggest that while the higher-order oligomers (multimer and polymer) of BclXL display some degree of polydispersity ($M_w/M_n > 1.05$) under all pH conditions (pH 6–10) where they are observed, the monomeric and dimeric forms of BclXL are predominantly monodisperse ($M_w/M_n < 1.05$). Strikingly, BclXL not only exclusively exists as a megadalton oligomer under acidic conditions (pH 4) but it also surprisingly appears to be highly monodisperse ($M_w/M_n < 1.05$). Additionally, the higher-order oligomers (multimer and polymer) of BclXL most likely adopt an elongated rod-like shape ($R_g/R_h > 1.05$) in lieu of a more spherical or disc-like architecture and such quaternary topology seems to be somewhat more favored at pH 6 than under alkaline conditions (pH 8 and pH 10). Consistent with these observations, the megamer observed at pH 4 also seems to adopt an highly elongated rod-like topology ($R_g/R_h > 2$) with a radius of gyration of ~100 nm, arguing that it may bear the propensity to assemble into fibrils of up to hundreds of nm in length in a manner akin to amyloid fibrils. Indeed, in a recent development, BclXL was shown to aggregate into amyloid-like fibrils under elevated temperatures [64].

pH destabilizes structure and stability of BclXL

Given that acidic pH promotes the association of BclXL into a megadalton oligomer, we next analyzed the effect of solution pH on the stability of this key apoptotic regulator using DSC (Fig. 3a). Consistent with our ALS analysis, our data reveal that

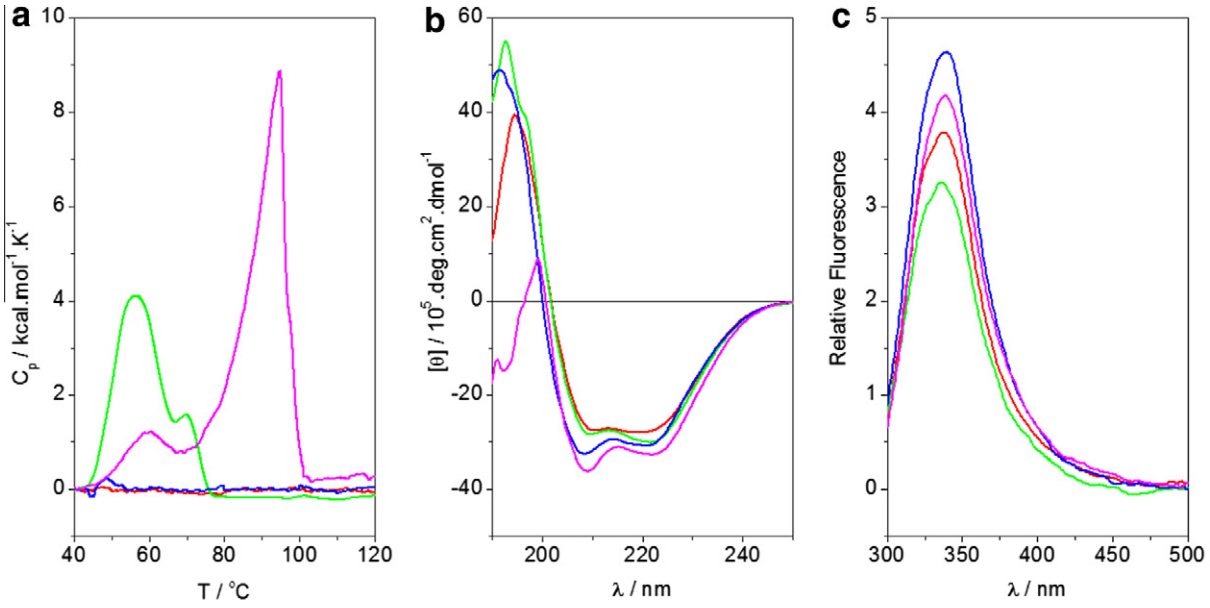

Fig. 3. Structure and stability of full-length BclXL monitored at pH 4 (red), pH 6 (green), pH 8 (blue) and pH 10 (magenta) using various techniques. (a) DSC isotherms of BclXL at various pH. (b) Far-UV CD spectra of BclXL at various pH. (c) SSF spectra of BclXL at various pH. (For interpretation of the references to colour in this figure legend, the reader is referred to the web version of this article.)

BclXL is extremely stable under acidic conditions (pH 4) and does not undergo a melting transition even when the temperature is raised to 120 °C. As the pH is raised to 6, BclXL exhibits two thermal phases with melting temperature (T_m) of around 55 °C and 70 °C in agreement with the observation that it exists in an equilibrium between various oligomeric states. We attribute these transitions to the dissociation of BclXL dimer (55 °C) into monomers and the subsequent unfolding of these monomers (70 °C). Interestingly, the thermal stability of BclXL at pH 8 is indistinguishable from that observed at pH 4, implying that although BclXL does not associate into a 1000-mer observed at pH 4, the much smaller oligomeric species observed at pH 8 are nonetheless highly stable. Finally, melting of BclXL at pH 10 is characterized by two distinct thermal phases accompanied by T_m values of around 60 °C and 90 °C, which most likely correspond to the dissociation of BclXL dimer into monomers and the subsequent unfolding of these monomers, respectively. Collectively, our DSC data suggest that although BclXL bears the propensity to associate into higher-order oligomers under all pH conditions, the oligomers observed at pH 6 and pH 10 are thermally much less stable than those observed at pH 4 and pH 8. We also note that the above findings were further confirmed by thermal denaturation curves obtained for BclXL under various pH conditions using far-UV CD (data not shown).

Next, we wondered whether differential stability of BclXL under various pH conditions also correlates with its structure. Toward this goal, we first measured far-UV CD spectra of full-length BclXL to probe the secondary structure as a function of pH (Fig. 3b). Notably, BclXL displays spectral features in the far-UV region characteristic of an α-helical fold with bands centered around 208 nm and 222 nm under all pH conditions. However, there are subtle differences that offer us a key glimpse into how pH affects protein secondary structure. Thus, the intensity of the far-UV spectrum of BclXL steadily increases with increasing pH, implying that the protein has a higher propensity to adopt α-helical fold under alkaline than acidic conditions. We believe that such decrease in α-helical propensity as the pH decreases likely underscores its ability to associate into a megadalton oligomer at pH 4. Spurred on by these promising insights, we also conducted SSF analysis on full-length BclXL to monitor tertiary and quaternary structural changes accompanying BclXL as a function of pH (Fig. 3c). It is important to note that intrinsic protein fluorescence, largely due to tryptophan residues, is influenced by changes in the local environment and thus serves as a sensitive probe of overall conformational changes within proteins. This is further aided by the fact that there are seven tryptophan residues within BclXL, located at various strategic positions to monitor conformational changes occurring at both the intramolecular and intermolecular level.

In agreement with foregoing argument, our SSF analysis shows that the intrinsic fluorescence of BclXL is highly pH-dependent, implying that protein tertiary and quaternary structures are perturbed by solution pH. Thus, while intrinsic fluorescence of BclXL drops as the pH changes from 4 to 6, it undergoes substantial enhancement at pH 8 only to drop again at pH 10. The enhancement in intrinsic fluorescence is most likely due to the transfer of tryptophan residues to a more hydrophobic environment, while a drop in intrinsic fluorescence could be explained by the greater solvent-exposure of tryptophan residues. Accordingly, one plausible interpretation of these subtle changes in intrinsic fluorescence is that the protein tertiary and quaternary structures experience largest perturbation at pH 6, while experiencing less perturbation at other pH conditions. However, we note that the presence of several tryptophan residues within BclXL may mask and average out the changes in intrinsic fluorescence observed here instead of providing a site-specific information. This argument is further supported by the fact that the tryptophan emission maximum observed in BclXL lies around 338 nm and does not appear to be pH-dependent. It should be noted that the tryptophan emission maximum is highly sensitive to the polarity of the surrounding solvent environment and occurs around 350 nm when fully exposed to water and around 330 nm when fully buried within the hydrophobic core of a protein. Thus, a value of 338 nm observed for the tryptophan emission maximum in BclXL most likely arises from an averaging effect and suggests that while some tryptophan residues may be fully buried within the interior of the protein, others are

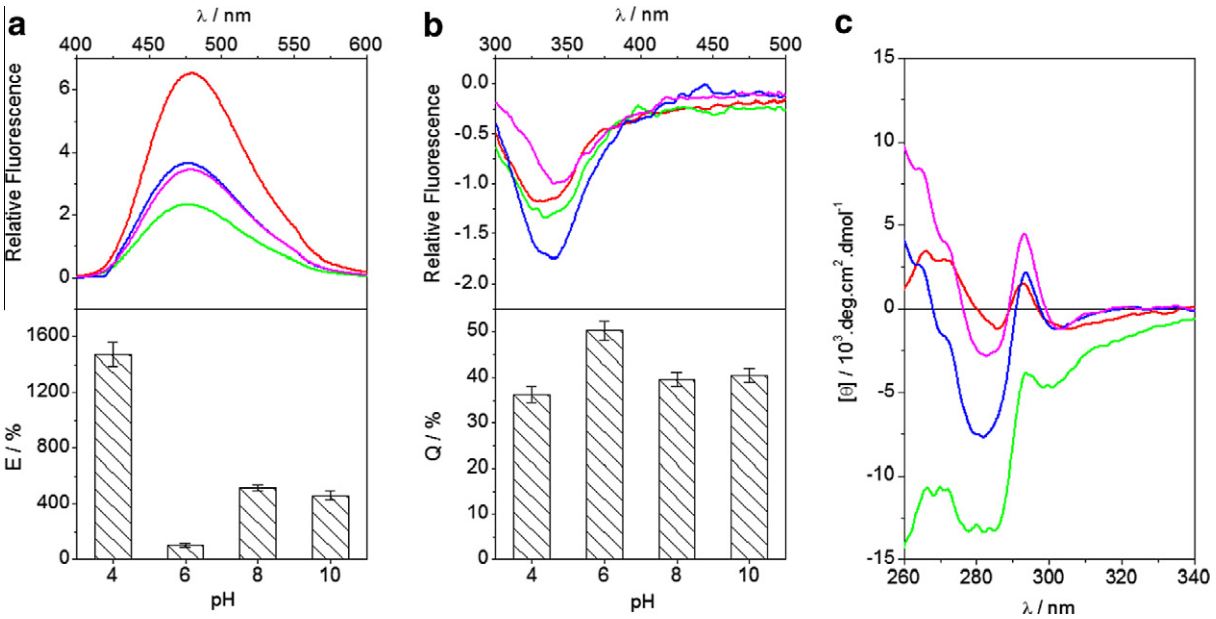

Fig. 4. Tertiary structural analysis of full-length BclXL at pH 4 (red), pH 6 (green), pH 8 (blue) and pH 10 (magenta) using various techniques. (a) SSF spectra of ANS in the presence of BclXL at various pH. (b) SSF spectra of BclXL in the presence of excess acrylamide at various pH. (c) Near-UV CD spectra of BclXL alone at various pH. Note that the background fluorescence due to ANS alone (a) and BclXL alone (b) was subtracted from the spectra shown at each pH. In (a) and (b), the upper panels show raw SSF spectra, while corresponding fluorescence enhancement (E) and fluorescence quenching (Q) at each pH are displayed in the lower panels. (For interpretation of the references to colour in this figure legend, the reader is referred to the web version of this article.)

likely to be solvent-exposed. We note that the tryptophan emission can also be influenced by resonance energy transfer from nearby tyrosine residues. In particular, tyrosine residues within BclXL are likely to exist in the negatively-charged phenolate state due to the ionization of the sidechain hydroxyl moiety at pH 10. Accordingly, changes in the ionization state of neighboring tyrosine residues as the solution pH varies must also influence the intrinsic fluorescence of tryptophan residues in a highly subtle manner. Despite these caveats, the data presented above are consistent with the propensity of BclXL to undergo oligomerization and its affinity toward Bid_BH3 peptide as a function of pH.

Acidic pH induces the formation of molten globule and promotes membrane insertion of BclXL

Acidic pH is believed to destabilize the solution conformation of bacterial toxins while at the same time inducing the formation of molten globule, which is believed to serve as an intermediate for subsequent insertion into membranes [27,11,28,29]. We wondered whether the propensity of BclXL to associate into a megadalton oligomer with a rod-like appearance at pH 4 also manifests in the formation of a molten globule. To test this hypothesis, we determined the effect of binding of ANS to BclXL as a function of pH using SSF (Fig. 4a). ANS is a hydrophobic fluorescent dye whose fluorescence undergoes substantial enhancement upon binding to exposed apolar surfaces such as those characteristic of molten globule conformations of proteins [65]. More importantly, ANS has been widely used as a test for the demonstration of molten globule-like states in proteins. Consistent with this notion, our data show that in the presence of BclXL, ANS experiences close to 15-fold fluorescence enhancement at pH 4 versus a mere 2-fold at pH 6, while under alkaline conditions (pH 8 and 10), its fluorescence undergoes about 5-fold enhancement. That this is so strongly suggests that acidic pH induces the formation of molten globule within BclXL and that megadalton oligomer observed here may be an on-pathway intermediate primed for insertion into MOM in response to apoptotic cues. This salient observation is in remarkable agreement with the evidence that upon apoptotic induction, a pH gradient is formed across the mitochondria with alkalinization of mitochondrial matrix and acidification of the cytosol [34–39]. We also note that while ANS emission occurs maximally around 515 nm in water, it appears to be blue-shifted to around 475 nm upon binding to BclXL. This is further evidence for the exposure of hydrophobic surfaces in BclXL under all pH conditions, albeit more so at pH 4.

To further test the notion that pH modulates tertiary and quaternary structure of BclXL, we also monitored the extent of quenching of intrinsic tryptophan fluorescence by acrylamide using SSF (Fig. 4b). In this assay, the extent of quenching directly correlates with the degree of solvent-exposure of tryptophan residues within a protein. As mentioned earlier, BclXL is decorated with seven tryptophan residues located at various strategic positions to monitor conformational changes occurring at both the intramolecular and intermolecular level. As shown in Fig. 4b, our fluorescence quenching analysis with acrylamide reveals that the optimal quenching occurs at pH 6, implying that the tryptophan residues either undergo some level of burial or dehydration under acidic as well as alkaline conditions. These data thus strongly argue that BclXL is characterized by the solvent-exposure of apolar surfaces in a manner akin to a molten globule under acidic conditions, while changes in pH result in perturbation of tertiary and quaternary structure as monitored by the movement of tryptophan residues. This notion is further corroborated by our near-UV CD analysis (Fig. 4c), which largely monitors the chiral environment of aromatic residues such as tryptophan and tyrosine. Thus, while BclXL exhibits a strong near-UV CD signal at pH 6, it becomes substantially attenuated under acidic pH. This implies that BclXL loses substantial tertiary structure under acidic conditions in agreement with our view that acidic pH induces the formation of molten globule. Interestingly, the near-UV CD signal is also attenuated under alkaline conditions (pH 8 and 10), arguing that not only acidic but also alkaline pH destabilizes the tertiary structure of BclXL.

To test our hypothesis that the molten globule-like state of BclXL observed under acidic pH may serve as an intermediate for membrane insertion, we next directly analyzed the binding of BclXL to mixed TOCL/DHPC bicelles as a function of pH using ITC (Fig. 5 and Table 3). Our analysis reveals that BclXL binds to TOCL/DHPC bicelles, used here as a model for MOM, only under acidic conditions. Importantly, varying the conditions of ITC experiments such as temperature or ionic strength had no effect on these

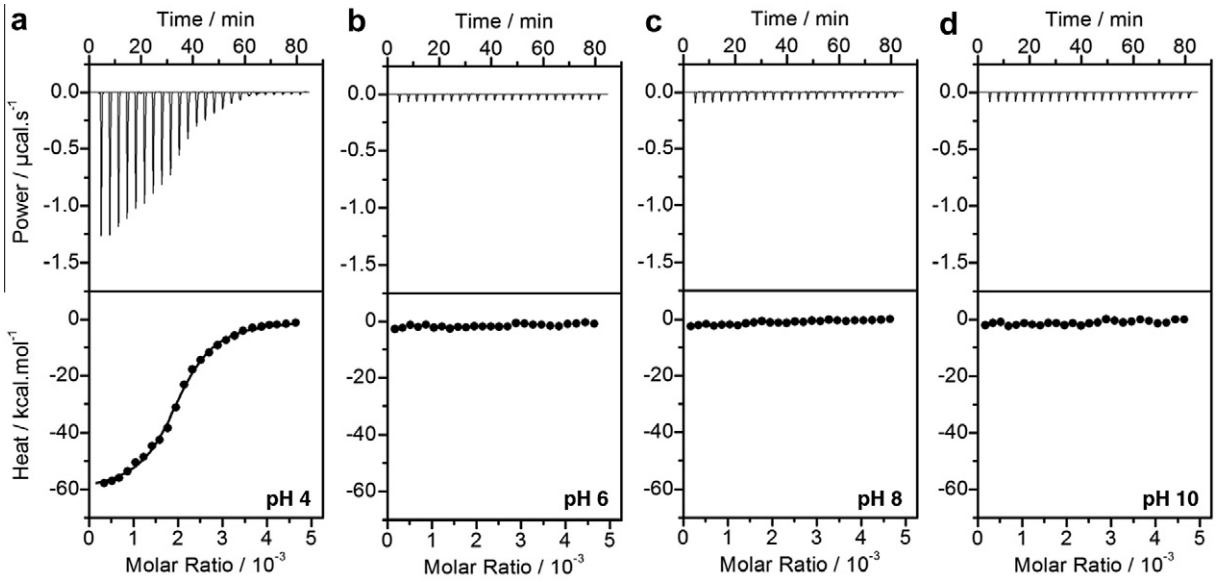

Fig. 5. ITC analysis for the binding of full-length BclXL to mixed TOCL/DHPC bicelles at pH 4 (a), pH 6 (b), pH 8 (c) and pH 10 (d). The upper panels show raw ITC data expressed as change in thermal power with respect to time over the period of titration. In the lower panels, change in molar heat is expressed as a function of molar ratio of BclXL to bicelles. In (a), the solid line in the lower panel shows non-linear least squares fit of data to a one-site binding model using the ORIGIN software as described earlier [40].

Table 3
pH-dependence of thermodynamic parameters for the binding of full-length BclXL to mixed TOCL/DHPC bicelles.

	K_d (μM)	ΔH (kcal mol^{-1})	$T\Delta S$ (kcal mol^{-1})	ΔG (kcal mol^{-1})
pH 4	0.17 ± 0.02	−63.00 ± 4.2	−53.73 ± 4.1	−9.26 ± 0.1
pH 6	NB	NB	NB	NB
pH 8	NB	NB	NB	NB
pH 10	NB	NB	NB	NB

All parameters were obtained from ITC measurements. Errors were calculated from at least three independent measurements. All errors are given to one standard deviation. NB indicates no binding observed.

observations, implying that BclXL indeed bears intrinsic affinity for bicelles only under acidic pH in lieu of lack of any observable change in the heat of binding, a scenario that may prevail for macromolecular interactions under entropic control. Notably, the truncation of the C-terminal TM domain completely abolished the binding of BclXL to bicelles under all pH conditions (data not shown), implying that the TM domain is a requisite for membrane insertion of BclXL. This salient observation is consistent with previous developments implicating the role of TM domain in mediating membrane insertion of apoptotic repressors [66–68], but contrasts other studies where regions other than the TM domain have been suggested [69,70]. More importantly, the observation that the truncation of TM domain in both BclXL and Bcl2 repressors renders them cytosolic and impairs their ability to prevent apoptotic cell death may be due to their inability to insert into MOM upon apoptotic induction [71,67]. We note that while TOCL only comprises about 10% of total phospholipid content of MOM, it is believed to be critical for the mitochondrial targeting of apoptotic regulators and the subsequent release of apoptogenic factors such as cytochrome *c* [72–76]. This is largely due to the highly distinguished structural features of TOCL. Thus, unlike canonical phospholipids, TOCL is a diphospholipid wherein two phosphatidylglycerols connect with a central glycerol backbone to form a dimeric structure. Importantly, the tetraoleoyl fatty acid moieties combined with an acidic head group in TOCL provide a unique chemical and structural configuration for the interaction of MOM with apoptotic regulators and other mitochondrial proteins in a highly specific manner. It is also noteworthy that artificial membranes, such as bicelles and liposomes, devoid of TOCL display little or no affinity toward apoptotic regulators [77–80].

Ligand binding and membrane insertion are coupled to conformational changes within BclXL

To further shed light on the propensity of BclXL to oligomerize in solution, we conducted SEM analysis as a function of pH on

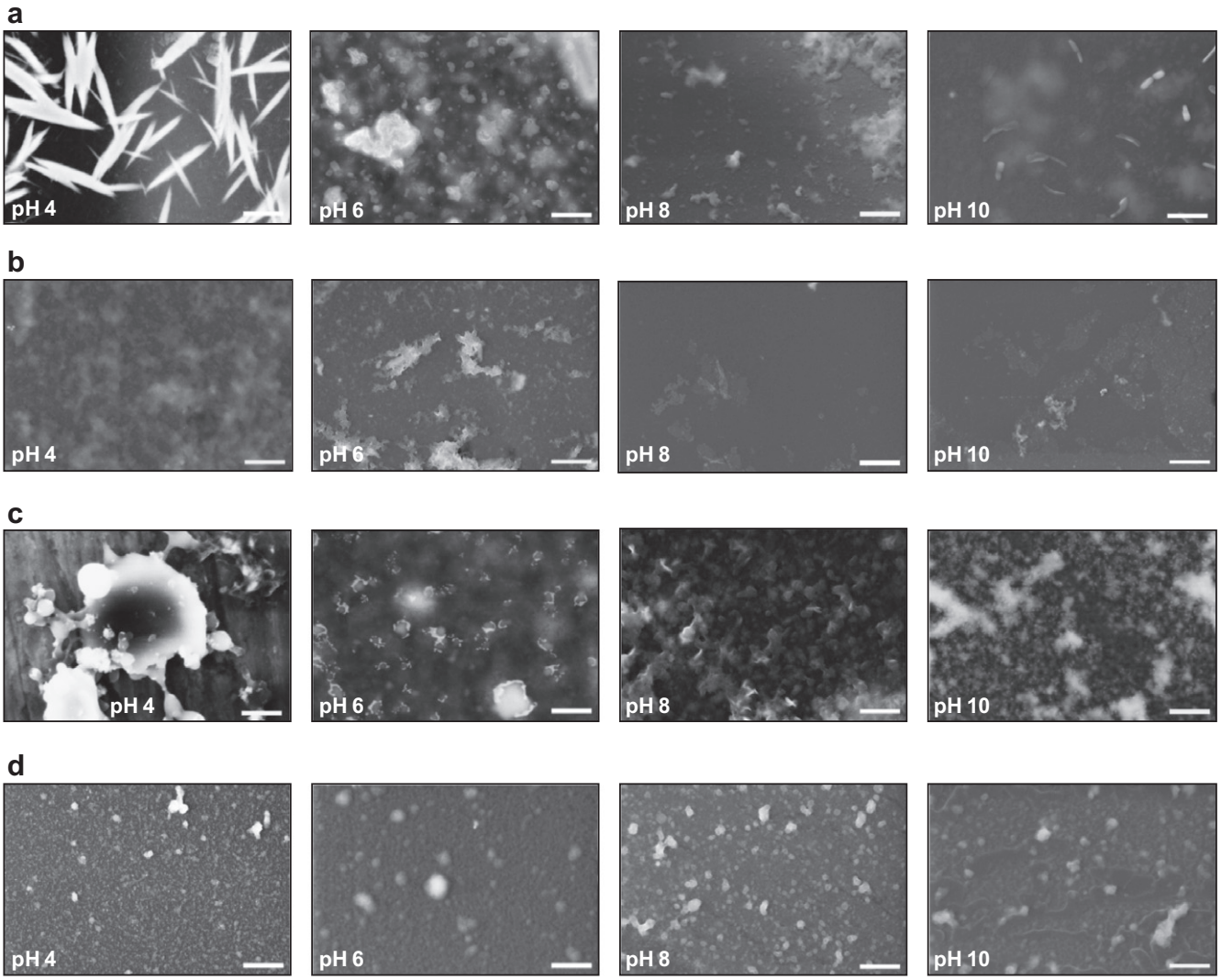

Fig. 6. SEM micrographs of full-length BclXL alone (a), BclXL in the presence of excess Bid_BH3 peptide (b), BclXL in the presence of excess TOCL/DHPC bicelles (c), and TOCL/DHPC bicelles alone (d) under various pH conditions as indicated. The scale bar represents 1 μm.

full-length BclXL alone, in the presence of Bid_BH3 peptide and in the presence of mixed TOCL/DHPC bicelles as a mimetic for MOM (Fig. 6). Consistent with our ALS analysis, our SEM data reveal that BclXL assembles into plume-like soluble aggregates with lengths of up to a few μm at pH 4 (Fig. 6a). In contrast, BclXL adopts poorly-defined amorphous structures at pH 6 and pH 8, while much smaller rod-like aggregates are observed at pH 10. Remarkably, the soluble aggregates of BclXL undergo conformational change and appear to dissociate into much smaller oligomers upon the addition of Bid_BH3 peptide under all pH conditions (Fig. 6b). This change is particularly striking at pH 4, implying that ligand binding and protein oligomerization occur in a competitive manner as reported in our previous study [40]. In a manner akin to ligand binding, the interaction of BclXL with TOCL/DHPC bicelles also appears to dramatically perturb its solution conformation under all pH conditions (Fig. 6c and d). However, such solution–membrane transition is most notable at pH 4, where large plume-like aggregates transform into ring-like structures in association with bicelles, whereas interaction of BclXL is much less conspicuous under other pH conditions. The most straightforward interpretation of these data is that the binding of BclXL to bicelles occurs optimally at pH 4 in agreement with our SSF and ITC data presented above.

Structural models provide physical basis of acid-induced oligomerization of BclXL

In an effort to understand the physical basis of acid-induced oligomerization of full-length BclXL, we built structural models of BclXL in two distinct conformations, herein referred to as BclXL_transTM and BclXL_runawayTM (Fig. 7). In BclXL_transTM conformation, the TM domain of one monomer occupies the canonical hydrophobic groove within the other monomer and vice versa in a domain-swapped trans-fashion as described earlier [40]. In BclXL_runawayTM conformation, the TM domain of one monomer occupies the canonical hydrophobic groove within the

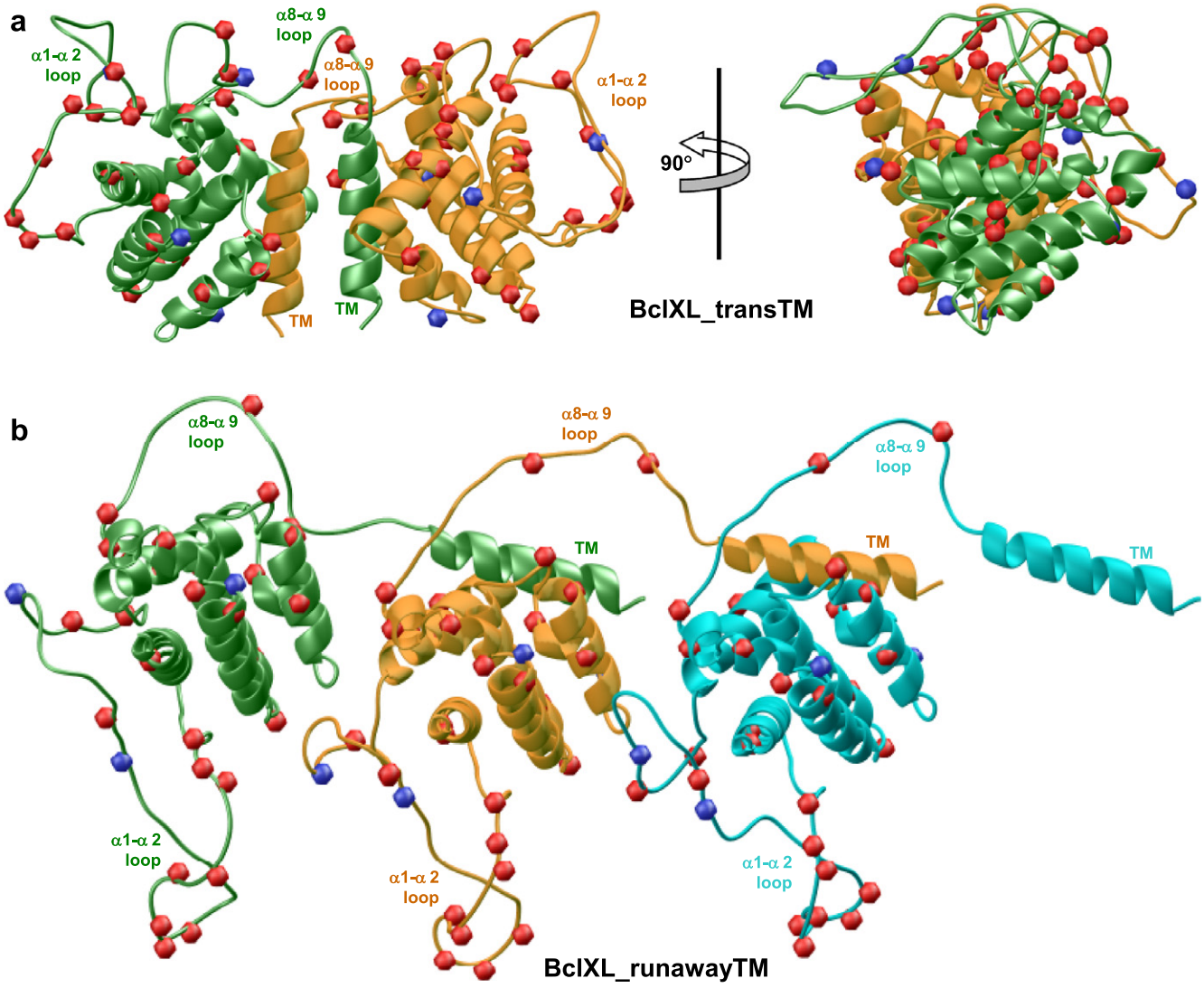

Fig. 7. Structural models of full-length BclXL in two distinct oligomeric conformations, herein designated BclXL_transTM (a) and BclXL_runawayTM (b). In BclXL_transTM conformation, the TM domain of one monomer (green) occupies the canonical hydrophobic groove within the other monomer (yellow) and vice versa in a domain-swapped trans-fashion. In BclXL_runawayTM conformation, the TM domain of one monomer (green) occupies the canonical hydrophobic groove within the adjacent monomer (yellow) and the TM domain of this second monomer (yellow) in turn occupies the canonical hydrophobic groove within the third monomer (cyan) in a runaway domain-swapping fashion. In each model, the red spheres denote the Cα atom of Asp/Glu residues and the blue spheres the Cα atom of His residues. Note also that the TM domain (α9 helix), α1–α2 loop and α8–α9 loop are labeled within each monomer. (For interpretation of the references to colour in this figure legend, the reader is referred to the web version of this article.)

adjacent monomer and the TM domain of this second monomer in turn occupies the canonical hydrophobic groove within the third monomer in a runaway domain-swapping fashion. It is noteworthy that these structural models were derived from the known solution structures of truncated BclXL, in which the TM domain and the α1–α2 loop are missing, and the full-length Bax in which the TM domain occupies the canonical hydrophobic groove [81,82]. As discussed earlier, the topological fold of BclXL is comprised of a central predominantly hydrophobic α-helical hairpin dagger (α5 and α6) surrounded by a cloak comprised of six amphipathic α-helices (α1–α4 and α7–α8) of varying lengths. However, the key to BclXL oligomerization appear to be the TM domain, which we believe undergoes domain swapping either in a trans-fashion (BclXL_transTM) or via the runaway mechanism (BclXL_runawayTM).

Over the past decade or so, oligomerization of proteins through domain-swapping has emerged as a common mechanism for the assembly of proteins into higher-order structures [83–88]. From a thermodynamic standpoint, such intermolecular association would allow two participating monomers to bury additional surface area culminating in not only enhanced stability but also providing a greater interacting molecular surface for further oligomerization. This could occur either through the formation of TM-swapped dimers (Fig. 7a), which would serve as building blocks for further oligomerization, or alternatively, the TM domain could promote oligomerization of BclXL in a head-to-tail fashion (Fig. 7b). More importantly, our structural models reveal that the surface of BclXL is heavily decorated with ionizable residues such as Asp, Glu and His, which are particularly prevalent in the α1–α2 loop. Accordingly, these ionizable residues must play a key role in the acid-induced association of BclXL into a megadalton oligomer observed here. Thus, under alkaline conditions, the deprotonation of these ionizable residues will likely increase overall negative charge on BclXL and the resulting electrostatic repulsions between neighboring residues may act as a barrier to extensive oligomerization observed at pH 4. On the other hand, under acidic conditions, protonation will result in the neutralization of negative charge on Asp/Glu residues, while His residues will gain a net positive charge. Such change in electrostatic polarity may not only promote association of BclXL into a megadalton oligomer observed here but would also likely render it thermodynamically more favorable for the protein to "breathe" and "open up" and, in so doing, facilitate the formation of a molten globule required for its insertion into membrane. It is also conceivable that one or more His residues may engage in some sort of ion pairing with Asp/Glu residues at pH 6, where His will be positively charged but Asp/Glu will bear a net negative charge, within BclXL in an intramolecular manner. Such charge-charge interactions could account for the rather low propensity of BclXL to undergo oligomerization at the expense of monomeric conformation at pH 6 (Fig. 2a). However, as the pH becomes more acidic, the neutralization of negative charge on Asp/Glu residues will disfavor such intramolecular ion pairing with His and may facilitate oligomerization as observed at pH 4. Importantly, such a scenario is plausible in light of our structural models. In particular, a pair of His residues located within the α1–α2 loop (H58/H71) lies within close proximity to D61/D76/E79, all of which would be negatively charged at pH 6.

We note that the oligomerization of RNase A through domain-swapping under acidic conditions has also been reported previously [86]. While such oligomerization of RNase A proceeds through an unfolded intermediate [89], we do not believe that a similar scenario also prevails in the case of BclXL oligomerization observed here under acidic conditions. This notion is primarily

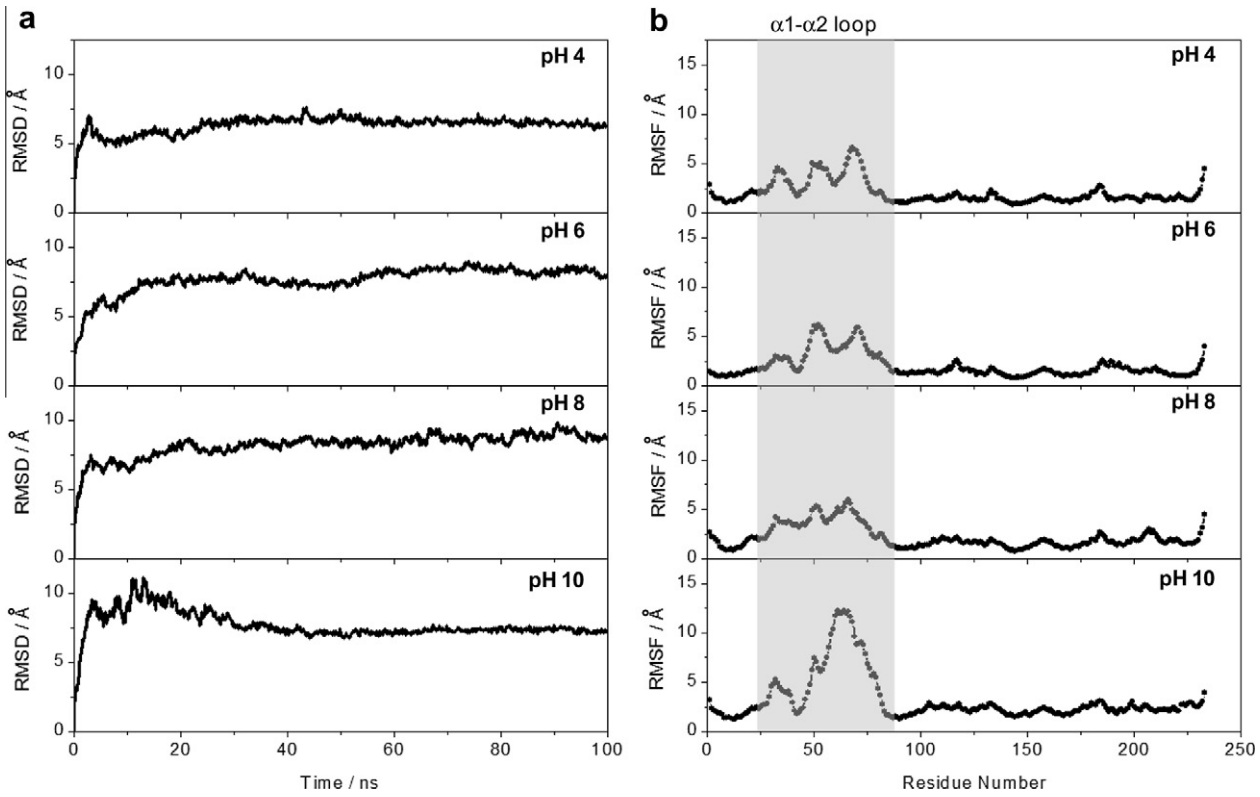

Fig. 8. MD analysis on the structural model of BclXL_transTM dimeric conformation as a function of pH. (a) Root mean square deviation (RMSD) of backbone atoms (N, Cα and C) within each simulated structure relative to the initial modeled structure of BclXL_transTM as a function of simulation time under various pH conditions as indicated. (b) Root mean square fluctuation (RMSF) of backbone atoms (N, Cα and C) averaged over the entire course of corresponding MD trajectory of BclXL_transTM as a function of residue number under various pH conditions as indicated. The shaded vertical rectangular box indicates the position of residues within the α1–α2 loop.

supported by our far-UV CD analysis wherein BclXL retains a native-like secondary structure under both acidic and alkaline conditions (Fig. 3b). Although the oligomerization of BclXL may not ensue via an unfolded intermediate, our studies strongly support the role of a molten globule intermediate in both the oligomerization and membrane insertion of BclXL.

MD simulations suggest that the atomic fluctuations within BclXL are pH-dependent

Our structural models of full-length BclXL presented above suggest strongly that the charged residues may play an active role in driving its association into a megadalton oligomer under acidic conditions. To test this hypothesis and to gain insights into macromolecular dynamics of BclXL as a function of pH, we conducted MD simulations on the BclXL_transTM dimeric conformation over tens of nanoseconds (Fig. 8). As shown in Fig. 8a, the MD trajectories reveal that while BclXL reaches structural equilibrium under near-neutral conditions (pH 6 and 8) after about 20 ns with an overall root mean square deviation (RMSD) of ~8 Å, its structural stability is highly compromised under both acidic (pH 4) and alkaline (pH 10) conditions within this time regime. In particular, the poor structural stability of BclXL at pH 4 may account for its ability to associate into higher-order oligomers such as the plume-like aggregates observed here. An alternative means to assess mobility and stability of macromolecular complexes is through an assessment of the root mean square fluctuation (RMSF) of specific atoms over the course of MD simulation. Fig. 8b provides such analysis for the backbone atoms of each residue within BclXL. The RMSF analysis reveals that while a majority of residues within BclXL appear to be well-ordered under all pH conditions, the residues within the α1–α2 loop experience rapid fluctuations which are particularly exaggerated at pH 10. Given that the α1–α2 loop is extensively decorated with acidic residues, it would be plausible to suggest that neutralization of negative charge within this loop under acidic pH may serve as a signal for the association of BclXL into a megadalton oligomer. It is noteworthy that the deletion of the α1- α2 loop in BclXL augments its anti-apoptogenicity and that the suppressive effect of α1–α2 loop is relieved by its post-translational phosphorylation [90]. In light of this observation, we believe that the intrinsic flexibility of the α1–α2 loop may be a driving force for the oligomerization of BclXL through favorable entropic contributions and that such intermolecular association most likely compromises its anti-apoptotic action.

Conclusions

Our earlier studies provided the evidence for the association of full-length BclXL into higher-order oligomers under mildly alkaline conditions [40]. In this study, we have demonstrated that the oligomerization of BclXL is highly pH-dependent and that under acidic conditions, it associates into a megadalton oligomer with a plume-like appearance and harboring molten globule characteristics. Although such acidic conditions are unlikely to be recapitulated globally within the milieu of the living cell, it is highly conceivable that changes in pH of a few units is norm within small localized microenvironments of the cytosol. Indeed, several lines of evidence suggest the formation of a pH gradient across the mitochondria, accompanied by the alkalinization of mitochondrial matrix and acidification of the cytosol, upon the induction of apoptosis [34–39]. Additionally, our data also reflect the fact that the acidic conditions employed here may also serve as a mimicry for cellular stress. The ability of BclXL to undergo acid-induced oligomerization is thus highly relevant to the situation in vivo. More importantly, previous studies suggest that the molten globule represents a thermodynamically favorable route for the membrane insertion of many other proteins that undergo solution–membrane transition [27,11,28,29]. Consistent with this notion, our data argue that BclXL interacts with cardiolipin bicelles optimally under acidic conditions, which favor both its oligomerization and the formation of a molten globule. It is noteworthy that cardiolipin is not only exclusively found within mitochondrial membranes but, upon apoptotic induction, BclXL specifically localizes at the MOM [91], presumably through a physical interaction with cardiolipin. Regardless of the in vivo mechanisms involved in the insertion of BclXL into MOM, the data presented here unequivocally demonstrate that acidic pH promotes the oligomerization of BclXL and that such propensity of BclXL to undergo oligomerization is likely to be relevant to its in vivo function.

Acknowledgments

This work was supported by the National Institutes of Health Grants R01-GM083897 (to A.F.) and R01-AG033719 (to I.K.L.), and funds from the USylvester Braman Family Breast Cancer Institute (to A.F.). C.B.M. is a recipient of a postdoctoral fellowship from the National Institutes of Health (Award# T32-CA119929).

References

[1] J.M. Adams, S. Cory, Science 281 (1998) 1322–1326.
[2] A. Gross, J.M. McDonnell, S.J. Korsmeyer, Genes Dev. 13 (1999) 1899–1911.
[3] S.J. Korsmeyer, Cancer Res. 59 (1999) 1693s–1700s.
[4] T. Kuwana, D.D. Newmeyer, Curr. Opin. Cell Biol. 15 (2003) 691–699.
[5] R.J. Youle, A. Strasser, Nat. Rev. Mol. Cell Biol. 9 (2008) 47–59.
[6] G. Dewson, R.M. Kluck, J. Cell Sci. 122 (2009) 2801–2808.
[7] J.E. Chipuk, T. Moldoveanu, F. Llambi, M.J. Parsons, D.R. Green, Mol. Cell 37 (2010) 299–310.
[8] L.M. Dejean, S.Y. Ryu, S. Martinez-Caballero, O. Teijido, P.M. Peixoto, K.W. Kinnally, Biochim. Biophys. Acta 1797 (2010) 1231–1238.
[9] J.E. Chipuk, J.C. Fisher, C.P. Dillon, R.W. Kriwacki, T. Kuwana, D.R. Green, Proc. Natl. Acad. Sci. USA 105 (2008) 20327–20332.
[10] J.E. Chipuk, D.R. Green, Trends Cell Biol. 18 (2008) 157–164.
[11] F.G. van der Goot, J.M. Gonzalez-Manas, J.H. Lakey, F. Pattus, Nature 354 (1991) 408–410.
[12] E. London, Biochim. Biophys. Acta 1113 (1992) 25–51.
[13] J.H. Lakey, F.G. van der Goot, F. Pattus, Toxicology 87 (1994) 85–108.
[14] S.L. Schendel, M. Montal, J.C. Reed, Cell Death Differ. 5 (1998) 372–380.
[15] S.D. Zakharov, W.A. Cramer, Biochim. Biophys. Acta 1565 (2002) 333–346.
[16] A.M. Petros, E.T. Olejniczak, S.W. Fesik, Biochim. Biophys. Acta 1644 (2004) 83–94.
[17] S. Krajewski, S. Tanaka, S. Takayama, M.J. Schibler, W. Fenton, J.C. Reed, Cancer Res. 53 (1993) 4701–4714.
[18] M. Gonzalez-Garcia, R. Perez-Ballestero, L. Ding, L. Duan, L.H. Boise, C.B. Thompson, G. Nunez, Development 120 (1994) 3033–3042.
[19] H. Zha, H.A. Fisk, M.P. Yaffe, N. Mahajan, B. Herman, J.C. Reed, Mol. Cell. Biol. 16 (1996) 6494–6508.
[20] S.W. Muchmore, M. Sattler, H. Liang, R.P. Meadows, J.E. Harlan, H.S. Yoon, D. Nettesheim, B.S. Chang, C.B. Thompson, S.L. Wong, S.L. Ng, S.W. Fesik, Nature 381 (1996) 335–341.
[21] B. Antonsson, F. Conti, A. Ciavatta, S. Montessuit, S. Lewis, I. Martinou, L. Bernasconi, A. Bernard, J.J. Mermod, G. Mazzei, K. Maundrell, F. Gambale, R. Sadoul, J.C. Martinou, Science 277 (1997) 370–372.
[22] A.J. Minn, P. Velez, S.L. Schendel, H. Liang, S.W. Muchmore, S.W. Fesik, M. Fill, C.B. Thompson, Nature 385 (1997) 353–357.
[23] S.L. Schendel, Z. Xie, M.O. Montal, S. Matsuyama, M. Montal, J.C. Reed, Proc. Natl. Acad. Sci. USA 94 (1997) 5113–5118.
[24] P.H. Schlesinger, A. Gross, X.M. Yin, K. Yamamoto, M. Saito, G. Waksman, S.J. Korsmeyer, Proc. Natl. Acad. Sci. USA 94 (1997) 11357–11362.
[25] G. Basanez, J. Zhang, B.N. Chau, G.I. Maksaev, V.A. Frolov, T.A. Brandt, J. Burch, J.M. Hardwick, J. Zimmerberg, J. Biol. Chem. 276 (2001) 31083–31091.
[26] A. Chenal, P. Savarin, P. Nizard, F. Guillain, D. Gillet, V. Forge, J. Biol. Chem. 277 (2002) 43425–43432.
[27] M.G. Blewitt, L.A. Chung, E. London, Biochemistry 24 (1985) 5458–5464.
[28] V.E. Bychkova, A.E. Dujsekina, S.I. Klenin, E.I. Tiktopulo, V.N. Uversky, O.B. Ptitsyn, Biochemistry 35 (1996) 6058–6063.
[29] M. Song, H. Shao, A. Mujeeb, T.L. James, W.L. Miller, Biochem. J. 356 (2001) 151–158.
[30] K. Kuwajima, Proteins 6 (1989) 87–103.
[31] O.B. Ptitsyn, R.H. Pain, G.V. Semisotnov, E. Zerovnik, O.I. Razgulyaev, FEBS Lett. 262 (1990) 20–24.
[32] O.B. Ptitsyn, Trends Biochem. Sci. 20 (1995) 376–379.
[33] O.B. Ptitsyn, Adv. Protein Chem. 47 (1995) 83–229.

[34] D. Perez-Sala, D. Collado-Escobar, F. Mollinedo, J. Biol. Chem. 270 (1995) 6235–6242.
[35] G.W. Meisenholder, S.J. Martin, D.R. Green, J. Nordberg, B.M. Babior, R.A. Gottlieb, J. Biol. Chem. 271 (1996) 16260–16262.
[36] I.J. Furlong, R. Ascaso, A. Lopez Rivas, M.K. Collins, J. Cell Sci. 110 (Pt 5) (1997) 653–661.
[37] C.M. Wolf, A. Eastman, Biochem. Biophys. Res. Commun. 254 (1999) 821–827.
[38] S. Matsuyama, J. Llopis, Q.L. Deveraux, R.Y. Tsien, J.C. Reed, Nat. Cell Biol. 2 (2000) 318–325.
[39] S. Matsuyama, J.C. Reed, Cell Death Differ. 7 (2000) 1155–1165.
[40] V. Bhat, C.B. McDonald, D.C. Mikles, B.J. Deegan, K.L. Seldeen, M.L. Bates, A. Farooq, J. Mol. Biol. 416 (2012) 57–77.
41 E. Gasteiger, C. Hoogland, A. Gattiker, S. Duvaud, M.R. Wilkins, R.D. Appel, A. Bairoch, in: J.M. Walker (Ed.), The Proteomics Protocols Handbook, Humana Press, Totowa, New Jersey, USA, 2005, pp. 571–607.
[42] T. Wiseman, S. Williston, J.F. Brandts, L.N. Lin, Anal. Biochem. 179 (1989) 131–137.
[43] B.H. Zimm, J. Chem. Phys. 16 (1948) 1093–1099.
[44] D.E. Koppel, J. Chem. Phys. 57 (1972) 4814–4820.
[45] B.J. Berne, R. Pecora, Dynamic Light Scattering, Wiley, New York, 1976.
[46] B. Chu, Laser Light Scattering: Basic Principles and Practice, Academic, Boston, 1991.
[47] P.J. Wyatt, Anal. Chim. Acta 272 (1993) 1–40.
[48] R. Koradi, M. Billeter, K. Wuthrich, J. Mol. Graph. 14 (1996) 51–55.
[49] M.A. Marti-Renom, A.C. Stuart, A. Fiser, R. Sanchez, F. Melo, A. Sali, Annu. Rev. Biophys. Biomol. Struct. 29 (2000) 291–325.
[50] M. Carson, J. Appl. Crystallogr. 24 (1991) 958–961.
[51] D. Van Der Spoel, E. Lindahl, B. Hess, G. Groenhof, A.E. Mark, H.J. Berendsen, J. Comput. Chem. 26 (2005) 1701–1718.
[52] B. Hess, J. Chem. Theory Comput. 4 (2008) 435–447.
[53] W.L. Jorgensen, J. Tirado-Rives, J. Am. Chem. Soc. 110 (1988) 1657–1666.
[54] G.A. Kaminski, R.A. Friesner, J. Tirado-Rives, W.L. Jorgensen, J. Phys. Chem. B 105 (2001) 6474–6487.
[55] K. Toukan, A. Rahman, Phys. Rev. B 31 (1985) 2643–2648.
[56] H.J.C. Berendsen, J.R. Grigera, T.P. Straatsma, J. Phys. Chem. 91 (1987) 6269–6271.
[57] T.A. Darden, D. York, L. Pedersen, J. Chem. Phys. 98 (1993) 10089–10092.
[58] B. Hess, H. Bekker, H.J.C. Berendsen, J.G.E.M. Fraaije, J. Comput. Chem. 18 (1997) 1463–1472.
[59] R. Lumry, S. Rajender, Biopolymers 9 (1970) 1125–1227.
[60] M.R. Eftink, A.C. Anusiem, R.L. Biltonen, Biochemistry 22 (1983) 3884–3896.
[61] A. Cooper, C.M. Johnson, J.H. Lakey, M. Nollmann, Biophys. Chem. 93 (2001) 215–230.
[62] K. Sharp, Protein Sci. 10 (2001) 661–667.
[63] E.B. Starikov, B. Norden, J. Phys. Chem. B 111 (2007) 14431–14435.
[64] A. Chenal, C. Vendrely, H. Vitrac, J.C. Karst, A. Gonneaud, C.E. Blanchet, S. Pichard, E. Garcia, B. Salin, P. Catty, D. Gillet, N. Hussy, C. Marquette, C. Almunia, V. Forge, J. Mol. Biol. 415 (2012) 584–599.
[65] G.V. Semisotnov, N.A. Rodionova, O.I. Razgulyaev, V.N. Uversky, A.F. Gripas, R.I. Gilmanshin, Biopolymers 31 (1991) 119–128.
[66] M.G. Hinds, M. Lackmann, G.L. Skea, P.J. Harrison, D.C. Huang, C.L. Day, EMBO J. 22 (2003) 1497–1507.
[67] S.Y. Jeong, B. Gaume, Y.J. Lee, Y.T. Hsu, S.W. Ryu, S.H. Yoon, R.J. Youle, EMBO J. 23 (2004) 2146–2155.
[68] A. Ospina, A. Lagunas-Martinez, J. Pardo, J.A. Carrodeguas, FEBS Lett. 585 (2011) 2935–2942.
[69] C.M. Franzin, J. Choi, D. Zhai, J.C. Reed, F.M. Marassi, Magn. Reson. Chem. 42 (2004) 172–179.
[70] G.R. Thuduppathy, O. Terrones, J.W. Craig, G. Basanez, R.B. Hill, Biochemistry 45 (2006) 14533–14542.
[71] M. Nguyen, P.E. Branton, P.A. Walton, Z.N. Oltvai, S.J. Korsmeyer, G.C. Shore, J. Biol. Chem. 269 (1994) 16521–16524.
[72] M. Schlame, D. Rua, M.L. Greenberg, Prog. Lipid Res. 39 (2000) 257–288.
[73] M.D. Esposti, Cell Death Differ. 9 (2002) 234–236.
[74] T.H. Kim, Y. Zhao, W.X. Ding, J.N. Shin, X. He, Y.W. Seo, J. Chen, H. Rabinowich, A.A. Amoscato, X.M. Yin, Mol. Biol. Cell 15 (2004) 3061–3072.
[75] F. Gonzalvez, J.J. Bessoule, F. Rocchiccioli, S. Manon, P.X. Petit, Cell Death Differ. 12 (2005) 659–667.
[76] F. Gonzalvez, F. Pariselli, P. Dupaigne, I. Budihardjo, M. Lutter, B. Antonsson, P. Diolez, S. Manon, J.C. Martinou, M. Goubern, X. Wang, S. Bernard, P.X. Petit, Cell Death Differ. 12 (2005) 614–626.
[77] M. Lutter, M. Fang, X. Luo, M. Nishijima, X. Xie, X. Wang, Nat. Cell Biol. 2 (2000) 754–761.
[78] M.D. Esposti, I.M. Cristea, S.J. Gaskell, Y. Nakao, C. Dive, Cell Death Differ. 10 (2003) 1300–1309.
[79] A.J. Garcia-Saez, J. Ries, M. Orzaez, E. Perez-Paya, P. Schwille, Nat. Struct. Mol. Biol. 16 (2009) 1178–1185.
[80] F. Gonzalvez, F. Pariselli, O. Jalmar, P. Dupaigne, F. Sureau, M. Dellinger, E.A. Hendrickson, S. Bernard, P.X. Petit, PLoS ONE 5 (2010) e9342.
[81] M. Sattler, H. Liang, D. Nettesheim, R.P. Meadows, J.E. Harlan, M. Eberstadt, H.S. Yoon, S.B. Shuker, B.S. Chang, A.J. Minn, C.B. Thompson, S.W. Fesik, Science 275 (1997) 983–986.
[82] M. Suzuki, R.J. Youle, N. Tjandra, Cell 103 (2000) 645–654.
[83] M.J. Bennett, S. Choe, D. Eisenberg, Proc. Natl. Acad. Sci. USA 91 (1994) 3127–3131.
[84] R. Janowski, M. Kozak, E. Jankowska, Z. Grzonka, A. Grubb, M. Abrahamson, M. Jaskolski, Nat. Struct. Biol. 8 (2001) 316–320.
[85] Y. Liu, D. Eisenberg, Protein Sci. 11 (2002) 1285–1299.
[86] Y. Liu, G. Gotte, M. Libonati, D. Eisenberg, Protein Sci. 11 (2002) 371–380.
[87] M.J. Bennett, M.R. Sawaya, D. Eisenberg, Structure 14 (2006) 811–824.
[88] A.P. Benfield, B.B. Whiddon, J.H. Clements, S.F. Martin, Arch. Biochem. Biophys. 462 (2007) 47–53.
[89] J.P. Lopez-Alonso, M. Bruix, J. Font, M. Ribo, M. Vilanova, M.A. Jimenez, J. Santoro, C. Gonzalez, D.V. Laurents, J. Am. Chem. Soc. 132 (2010) 1621–1630.
[90] B.S. Chang, A.J. Minn, S.W. Muchmore, S.W. Fesik, C.B. Thompson, EMBO J. 16 (1997) 968–977.
[91] T. Kaufmann, S. Schlipf, J. Sanz, K. Neubert, R. Stein, C. Borner, J. Cell Biol. 160 (2003) 53–64.